Hyaluronan/collagen hydrogels containing sulfated hyaluronan improve wound healing by sustained release of Heparin-Binding EGF-like growth factor

Article *in* Acta Biomaterialia · January 2019

DOI: 10.1016/j.actbio.2019.01.029

CITATIONS
0

READS
84

14 authors, including:

Stephan Thönes
University of Leipzig
8 PUBLICATIONS **60** CITATIONS
SEE PROFILE

Sandra Rother
Technische Universität Dresden
27 PUBLICATIONS **111** CITATIONS
SEE PROFILE

Balamurugan Kanagasabai
Technische Universität Dresden
25 PUBLICATIONS **369** CITATIONS
SEE PROFILE

Stephanie Möller
INNOVENT e.V.
87 PUBLICATIONS **1,154** CITATIONS
SEE PROFILE

Acta Biomaterialia 86 (2019) 135–147

Contents lists available at ScienceDirect

Acta Biomaterialia

journal homepage: www.elsevier.com/locate/actabiomat

Full length article

Hyaluronan/collagen hydrogels containing sulfated hyaluronan improve wound healing by sustained release of heparin-binding EGF-like growth factor

Stephan Thönes [a,1], Sandra Rother [b,1], Tom Wippold [a,1], Joanna Blaszkiewicz [c], Kanagasabai Balamurugan [d], Stephanie Moeller [e], Gloria Ruiz-Gómez [d], Matthias Schnabelrauch [e], Dieter Scharnweber [b], Anja Saalbach [a], Joerg Rademann [c], M. Teresa Pisabarro [d], Vera Hintze [b,1], Ulf Anderegg [a,1,*]

[a] Department of Dermatology, Venereology and Allergology, Leipzig University, Johannisallee 30, 04103 Leipzig, Germany
[b] Institute of Materials Science, Max Bergmann Center of Biomaterials, TU Dresden, Budapester Strasse 27, 01069 Dresden, Germany
[c] Institute of Pharmacy, Medicinal Chemistry, Freie Universität Berlin, Königin-Luise-Strasse 2+4, 14195 Berlin, Germany
[d] Structural Bioinformatics, BIOTEC TU Dresden, Tatzberg 47-51, Dresden 01307, Germany
[e] Biomaterials Department, INNOVENT e.V., Prüssingstrasse 27B, 07745 Jena, Germany

ARTICLE INFO

Article history:
Received 27 August 2018
Received in revised form 8 January 2019
Accepted 14 January 2019
Available online 17 January 2019

Keywords:
Hyaluronan
Sulfated hyaluronan
Hydrogel
Heparin-binding epidermal growth factor-like growth factor (HB-EGF)
Extracellular matrix (ECM)
Biomimetic material
Surface plasmon resonance
Fibroblasts
Wound healing

ABSTRACT

Functional biomaterials that are able to bind, stabilize and release bioactive proteins in a defined manner are required for the controlled delivery of such to the desired place of action, stimulating wound healing in health-compromised patients. Glycosaminoglycans (GAG) represent a very promising group of components since they may be functionally engineered and are well tolerated by the recipient tissues due to their relative immunological inertness.

Ligands of the Epidermal Growth Factor (EGF) receptor (EGFR) activate keratinocytes and dermal fibroblasts and, thus, contribute to skin wound healing. Heparin-binding EGF-like growth factor (HB-EGF) bound to GAG in biomaterials (e.g. hydrogels) might serve as a reservoir that induces prolonged activation of the EGF receptor and to recover disturbed wound healing.

Based on previous findings, the capacity of hyaluronan (HA) and its sulfated derivatives (sHA) to bind and release HB-EGF from HA/collagen-based hydrogels was investigated. Docking and molecular dynamics analysis of a molecular model of HB-EGF led to the identification of residues in the heparin-binding domain of the protein being essential for the recognition of GAG derivatives. Furthermore, molecular modeling and surface plasmon resonance (SPR) analyses demonstrated that sulfation of HA increases binding strength to HB-EGF thus providing a rationale for the development of sHA-containing hydrogels. In line with computational observations and in agreement with SPR results, gels containing sHA displayed a retarded HB-EGF release *in vitro* compared to pure HA/collagen gels. Hydrogels containing HA and collagen or a mixture with sHA were shown to bind and release bioactive HB-EGF over at least 72 h, which induced keratinocyte migration, EGFR-signaling and HGF expression in dermal fibroblasts. Importantly, hydrogels containing sHA strongly increased the effectivity of HB-EGF in inducing epithelial tip growth in epithelial wounds shown in a porcine skin organ culture model. These findings suggest that hydrogels containing HA and sHA can be engineered for smart and effective wound dressings.

Statement of Significance

Immobilization and sustained release of recombinant proteins from functional biomaterials might overcome the limited success of direct application of non-protected solute growth factors during the treatment of impaired wound healing.

We developed HA/collagen-based hydrogels supplemented with acrylated sulfated HA for binding and release of HB-EGF. We analyzed the molecular basis of HB-EGF interaction with HA and its chemical

Abbreviations: AC, acrylated; Coll, collagen; CS, chondroitin sulfate; DF, dermal fibroblasts; D.S., degree of substitution; D.U., disaccharide units; ECM, extracellular matrix; EGF, epidermal growth factor; EGFR, epidermal growth factor receptor; GAFF, General Amber Force Field; GAG, glycosaminoglycans; HA, hyaluronan; sHA, sulfated HA; HB, heparin binding; HB-EGF, heparin-binding EGF-like growth factor; HEP, Heparin; MD, molecular dynamics; PME, Particle Mesh Ewald; PDB, protein data bank; ps, persulfated.

* Corresponding author.
E-mail address: ulf.anderegg@medizin.uni-leipzig.de (U. Anderegg).
[1] Contributed equally.

https://doi.org/10.1016/j.actbio.2019.01.029

derivatives by *in silico* modeling and surface plasmon resonance. These hydrogels bind HB-EGF reversibly. Using different *in vitro* assays and organ culture we demonstrate that the introduction of sulfated HA into the hydrogels significantly increases the effectivity of HB-EGF action on target cells. Therefore, sulfated HA-containing hydrogels are promising functional biomaterials for the development of mediator releasing wound dressings.

1. Introduction

Glycosaminoglycans (GAG) are essential components of the extracellular matrix (ECM), being hyaluronan (HA) and dermatan sulfate the ones prevailing in skin. Therefore, they are highly biocompatible and are often used as basic constituents in designing biomaterials [1]. Native HA as non-sulfated GAG, or functionalized derivatives thereof are widely used as building blocks in regenerative medicine [2,3]. Especially HA derivatives with crosslinkable thiol or acrylate groups [4,5] are broadly used to generate three-dimensional structures [6]. Sulfated GAG like the naturally occurring chondroitin sulfate (CS) and heparan sulfate are structural and reservoir-forming matrix components of great physiologic relevance [7–9]. Especially the highly variable sulfation motifs of GAG direct the interactions with biological mediator proteins thereby regulating the cell behavior (so called "sulfation code" [10]). Recent developments in the design of functional biomaterials thus apply chemically sulfated GAG for tailoring interaction with cells [11].

EGFR-signaling is mandatory for the successful closure of skin wounds since these signals activate keratinocyte migration, proliferation and activate the underlying dermal fibroblasts. Moreover, first attempts using EGF proved the beneficial effects of EGFR ligands for the treatment of disturbed wound healing [12,13].

The EGFR's ligand HB-EGF potently supports migration and proliferation of keratinocytes [14–16], but its way of presentation determines whether migration (by immobilized HB-EGF) or proliferation (by solute HB-EGF) is supported [17,18]. Furthermore, HB-EGF induces the secretion of additional mediators by dermal fibroblasts that activate keratinocytes and have pro-angiogenic functions [19]. Beswick *et al.* reported an improved epithelial regeneration by HB-EGF in oral wound mouse models [20]. Occasionally, an advantage of HB-EGF over two other commonly used growth factors, namely fibroblast growth factor-2 (FGF2) and EGF was previously reported in healing studies [21,22]. HB-EGF specifically induces the phosphorylation of EGFR-Y1045 and activates Stat5, thus promoting cell proliferation and migration. The heparin-binding (HB) domain of HB-EGF is responsible for EGFR-mediated Stat5 activation, resulting in a more potent cellular proliferation and migration than that mediated by EGF [22].

Direct application of recombinant proteins to non-healing or burn wounds revealed to be ineffective due to short-lived activity and rapid degradation [23]. Therefore, intelligent delivery systems have to be developed which may preserve the integrity of the mediators in the wound milieu and release active compounds over longer time periods. Besides, the strategies of delivering proteins and other bioactive molecules in an encapsulated form, the application of hydrogels or other supporting materials that bind and release such molecules in a controlled fashion may be part of the solution and help to specifically improve healing of disturbed or very large wounds. The negatively charged nature of GAG molecules may facilitate the binding to positively charged residues in proteins or domains [24].

HB-EGF interacts via its HB domain with native GAG as part of proteoglycans located on the cell membrane and in the ECM [25,26]. Strong interaction with negatively charged GAG may be favorable for this molecule since bound HB-EGF may be retained within the GAG-containing matrix and released slowly over time, resulting in a long lasting local activity of HB-EGF.

In contrast to pure HA-based hydrogels which show poor cell attachment and quick enzymatic degradation [27], HA-based hydrogels incorporating collagen fibrils were reported to support endothelial cell growth and to be more stable against enzymatic degradation via hyaluronidase [28]. We aimed to analyze the interaction potential of HB-EGF with distinct chemically modified GAG derivatives. For this, HA-modified hydrogels were investigated towards their proposed capability to retain and slowly release active HB-EGF that might exert beneficial effects on cells being critical for skin wound healing. In case of large wounds (e.g. burns) or disturbed wound healing (e.g. diabetes, infection or chronic venous insufficiency), engineered hydrogels may provide fast and sterile wound closure and initiate endogenous wound repair. Hydrogels should form a beneficial micro-milieu that provides key functions of the natural extracellular environment supporting wound closure through migration and proliferation of the epidermal keratinocytes. We utilized a versatile HA/collagen-based hydrogel platform that can be independently adjusted with respect to mechanical and biochemical properties [28].

The effect of defined sulfation patterns and chain length of sulfated HA (sHA) derivatives on their interaction with HB-EGF in comparison to native HEP and CS were investigated via surface plasmon resonance (SPR). sHA was incorporated into the gels to increase the number of potential binding sites for growth factors, thus improving the binding and release characteristics for HB-EGF and, finally, the cellular response. In order to gain a deeper understanding on the experimentally observed binding and release, we carried out an atomic-detailed characterization of the interactions of HB-EGF with HA and sHA derivatives. For this, we established theoretical models based on computer-aided molecular modeling and dynamics simulation techniques. The results obtained from our computational and experimental binding studies help us to better understand GAG/HB-EGF molecular recognition and provide us with the rational basis for the development of improved new hydrogels.

The effects of the hydrogels on cells relevant for cutaneous wound healing were analyzed by *in vitro* studies using human and porcine dermal fibroblasts (DF), a human keratinocyte cell line (HaCat), and porcine skin organ culture.

2. Experimental section

2.1. Materials

Native HA (M_W = 1,100 kDa from *Streptococcus*) was purchased from Aqua Biochem (Dessau, Germany), CS (M_W = 20 kDa, 70% chondroitin-4-sulfate, 30% chrondroitin-6-sulfate, from porcine trachea) was from Kraeber (Ellerbek, Germany), sulfur trioxide/dimethylformamide complex (SO_3-DMF, active $SO_3 \geq 48\%$) and sulfur trioxide/pyridine complex (SO_3-pyridine, active $SO_3 \geq 45\%$) were obtained from FlukaChemie (Buchs, Switzerland). Rat collagen type I (coll) was received from Corning (Kaiserslautern,

Germany), HEP (M_W = 18 kDa, from porcine intestinal mucosa) and biochemical reagents were purchased from Sigma-Aldrich (Schnelldorf, Germany). Lithium phenyl-2,4,6-trimethylbenzoyl phosphinate (LAP) was obtained from TCI Deutschland GmbH (Eschborn, Germany) and human recombinant HB-EGF was from R&D Systems (Wiesbaden-Nordenstadt, Germany). CS- and HEP-hexasaccharides (degree of polymerization (dp) 6) were purchased from Iduron (Manchester, UK).

2.2. Preparation of GAG derivatives

Low-molecular weight HA, low-sulfated HA (sHA1) and differently sulfated HA oligosaccharides were synthesized and characterized as described earlier [29–33]. The influence of different sulfation patterns of HA on the interplay with HB-EGF was studied with a HA tetrasaccharide exclusively sulfated at the C6 position of the *N*-acetylglucosamine residues (sHA1 dp4), a sulfated derivative bearing no sulfate groups at the *N*-acetylglucosamine residues (sHA2Δ46s dp4), a HA tetrasaccharide fully sulfated at the glucuronic acid residues carrying one additional sulfate group at the C4 position of the *N*-acetylglucosamine residues (sHA3Δ6s dp4), and with per-sulfated HA tetra- and hexasaccharides, where all hydroxyl groups are substituted by sulfate groups (psHA dp4, dp6). Acrylated HA (HA-AC) and acrylated sHA1 (sHA1-AC) were prepared with acryloyl chloride according to previously described protocols [28]. The analytical characteristics of these GAG derivatives are reported in Table 1, while the structures of the studied HA oligosaccharide variants is displayed in Fig. 1(A–E).

2.3. Preparation of hydrogels

HA/collagen hydrogels with and without sHA1-AC were prepared as previously described [28]. In brief, 200 μL of HA-AC (10 mg/mL) dissolved in 0.5 mg/mL suspension of collagen type I fibrils were mixed with 20 μL LAP (1 mg/100 μL) dissolved in water. 200 μL of this mixture were filled into wells of a 48 well plate and photo-crosslinked with UV light (365 nm, 0.17 W/cm^2) for 600 s. HA-AC/sHA1-AC/coll gels were obtained by replacing 50 μL HA-AC by 50 μL of sHA1-AC (10 mg/mL) dissolved in 0.5 mg/mL suspension of collagen type I fibrils. Afterwards, the gels were lyophilized, washed twice with water, and lyophilized again.

The characterization of the hydrogels has been previously reported [28]. Scanning electron microscopy images proved the porous structure of the freeze-dried hydrogels with pore sizes of at least 100 μm. This porous structure with embedded collagen fibers was obtained irrespectively of the presence or absence of acrylated sulfated HA derivatives. Pure HA-AC/coll-based hydrogels showed an elastic modulus of 17 kPa ± 2 kPa, which is comparable to those containing additional sHA1-AC (16 kPa ± 1 kPa). However, the swelling ratio of the hydrogels differed depending on the composition. Both gel types bound more water than their initial dry weight within 5 min and gels with sHA1-AC absorbed even more water than pure HA-AC/coll hydrogels (swelling ratios of 47 ± 2 for HA-AC/coll and 74 ± 8 for HA-AC/sHA1-AC/coll). Both hydrogel types were biodegradable *in vitro* within 48 h by treatment with high hyaluronidase concentrations (1000 U/mL) [28].

2.4. Surface plasmon resonance measurements of HB-EGF interaction with GAGs

SPR studies were performed using a Biacore T100 instrument (GE Healthcare, USA) at 37 °C in HBS-EP running buffer (10 mM HEPES (pH 7.4), 150 mM NaCl, 3 mM EDTA, 0.05% surfactant P20). HB-EGF was immobilized on a CM5 Series S sensor chip (GE Healthcare) at 25 °C via amine coupling according to the manufacturer's protocol. An immobilization level of about 520 RU was

Table 1
Characterization of chemically modified HA derivatives. The respective degree of acrylation ($D.S._{AC}$) was estimated from ^{1}H NMR spectra, while the degree of sulfation ($D.S._S$) was calculated via the sulfur content determined with an elemental analyzer, the Mw was analyzed by gel permeation chromatography with laser light scattering detection. All sulfated oligohyaluronans are chromatographically pure compounds with fully assigned ^{1}H and ^{13}C NMR spectra; several compounds were confirmed by HRMS [30,31].

Sample	$D.S._S$	$D.S._{AC}$	Mw (kDa)
HA	–	–	48.26
HA-AC	–	0.6	145.68
CS	0.8	–	19.76
sHA1	1.2	–	26.42
sHA1-AC	1.5	0.7	27.01
HA (dp4)	–	–	0.78
sHA1 (dp4)	1.0	–	0.96
sHA2Δ46s (dp4)	2.0	–	1.36
sHA3Δ6s (dp4)	3.0	–	1.55
psHA (dp4)	4.0	–	1.76
psHA (dp6)	4.0	–	2.57

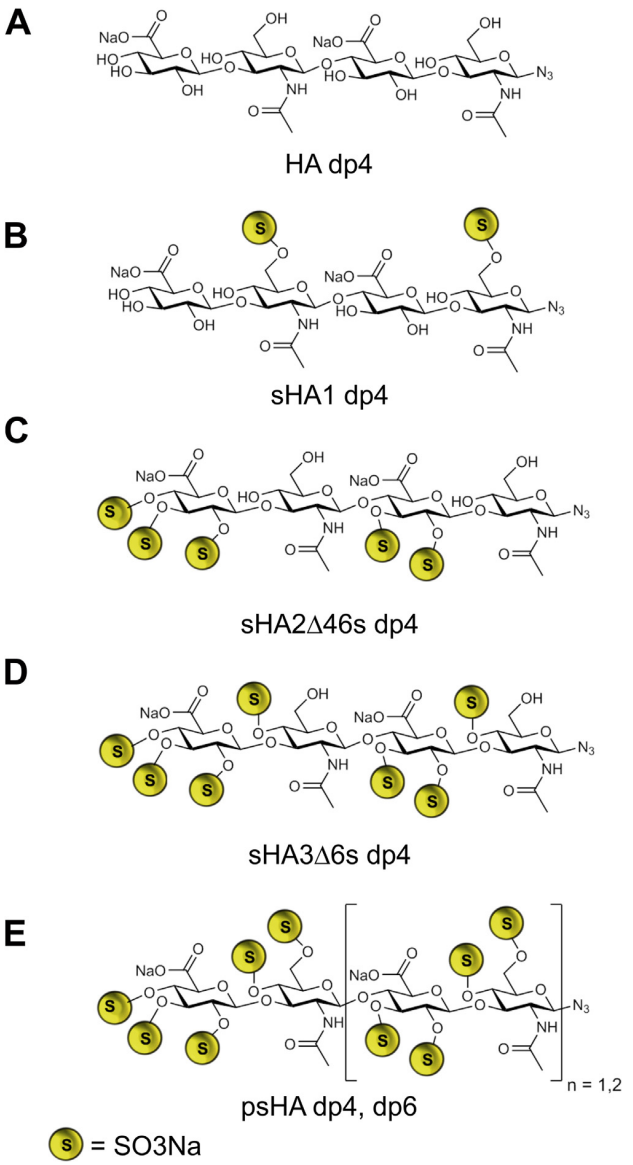

Fig. 1. Structure of analyzed HA and sHA oligosaccharides.

obtained after injection of HB-EGF (10 μg/mL) dissolved in sodium acetate buffer (pH 4.5) for 120 s at a flow rate of 5 μL/min. An activated and afterwards inactivated flow cell without immobilized

HB-EGF served as reference. For measurements of GAG binding to immobilized HB-EGF, GAG samples dissolved in running buffer to 1–400 μM disaccharide units were injected for 180 s at 30 μL/min. After each injection and a dissociation time of 600 s, the sensor chip surface was regenerated by injecting 5 M NaCl containing 5 mM NaOH for 60 s and allowed to stabilize for 1000 s. The signal from the experimental flow cell with immobilized HB-EGF was corrected by subtracting the signal from a buffer injection and the reference flow cell. The binding levels were recorded 10 s before the end of injection in order to rank the GAGs according to their binding strength. All measurements were performed in triplicate. The Biacore T100 evaluation software 2.03 was used to analyze the binding parameters.

2.5. Computational analysis of GAG/HB-EGF interactions

2.5.1. Modeling of HB-EGF

Fold recognition methods were used to predict the three-dimensional (3D) structure of the N-terminal region of HB-EGF (residues 1–44 from a total of 86). For this, the threading algorithm ProHit (ProCeryon Biosciences) [34,35] was employed as previously described [36]. The first 58 residues of HB-EGF were threaded against a fold library containing all protein structures currently available at the Protein Data Bank (PDB). Comparative modeling methods were applied to build the full structure of HB-EGF. The program Modeller implemented in Discovery Studio (Accelrys) [37] was used for this purpose. The top scoring hit resulting from the threading calculations (PDB-ID: 1ML4) [38] was used as template to model the N-terminal region. A high-resolution crystal structure containing an extracellular fragment of EGF in complex with diphtheria toxin (PDB-ID: 1XDT) [39] and a NMR structure consisting of an EGF-like domain (PDB_ID: 2RNL; model 16) were used as templates to model the rest of HB-EGF (residues 45–85 and 35–84 of HB-EGF, respectively). The resulting full structure of HB-EGF was energy refined by molecular dynamics (MD) in AMBER14 [40] (*vide infra;* Section 2.5.4). The lowest energy conformation was selected for further docking studies with the GAG derivatives.

2.5.2. Modeling of GAG derivatives

MOE (2016) [41] and AMBER14 [40] were used to model the following GAG molecules: tetrameric (dp 4) hyaluronan azide derivatives HA, sHA1, sHA3Δ6s, psHA, hexameric (dp 6) psHA, HA-AC and sHA1-AC (Fig. 1). Based on previous work [42], hexameric GAG length (dp6) was considered as representative of polymeric GAG for our docking studies.

2.5.3. Molecular docking

Binding of GAG derivatives to the modeled HB-EGF was analyzed by docking using Autodock 3 [43]. Autogrid 3 was used to calculate the atomic potential of each structure covering the full surface of HB-EGF with a grid box of 120 Å × 118 Å × 126 Å and a grid spacing of 0.447 Å. The GAG molecules were treated as completely flexible and the protein rigid. The Lamarckian genetic algorithm with an initial population size of 300 and a termination condition of 10,000 generations and 9.995×10^5 energy evaluations was used. A total of 1000 independent runs were carried out. Spatial clustering of the top 50 docking solutions was performed with the DBSCAN algorithm [44] as previously described [45]. For each GAG-protein system, a representative GAG binding pose was selected from the docking cluster obtained at the HB domain, and the corresponding complex was further refined by MD.

2.5.4. Molecular dynamics simulations

The GAG-protein complexes selected as representative from the docking studies were further refined by MD simulations in AMBER14 [40]. Charges were taken from the GLYCAM 06-j force field [46] for the different sulfated hyaluronan units and from the literature for sulfate groups [47]. AMM1-BCC charges [48] were used for the azide group. RESP atomic charges [49,50] were derived at the HF/6-31G(d) calculation level for the acrylate fragment using Gaussian09 [51]. Parameters for the GAG were taken from the GLYCAM-06j force field [46] and for the proteins from the ff14SB force field [40]. Missing parameters of the azide and acrylate groups were taken from the General Amber Force Field (GAFF) [52]. Each GAG-protein complex was solvated in a truncated octahedral box of TIP3P water molecules and neutralized with Na^+ or Cl^- counterions. MD simulations were preceded by two energy-minimization steps: *i)* only the solvent and ions were relaxed with position restraints for the solute (500 kcal/mol·Å^2) using 1000 steps of steepest descendent minimization followed by 500 steps of conjugate gradient minimization; *ii)* the entire system was minimized without restraints applying 3000 cycles of steepest descendent and 3000 steps of conjugate gradient equilibration. Then, the system was heated up from 200 K to 300 K in 20 ps with weak position restraints (10 kcal/mol·Å^2). Langevin temperature coupling with a collision frequency $\gamma = 1$ ps^{-1} was used at this step. The system was equilibrated under constant pressure of 1 atm using periodic boundary conditions (NPT conditions) at 300 K for 50 ps. A total of 50 ns MD simulation was carried out at 300 K NPT conditions for each complex. The SHAKE algorithm was used to constrain all bonds involving hydrogen atoms. A time step of 2 fs was used during SHAKE algorithm. A cutoff of 8 Å was applied to treat the non-bonded interactions and the Particle Mesh Ewald (PME) method was used to treat long-range electrostatic interactions. MD trajectories were recorded every 10 ps. The pyranose rings in the GAG molecules were harmonically restrained. Trajectories were visualized with VMD [53]. Energy decomposition per residue as well as binding free energy post-processing analysis of the last 300 frames from the MD simulations were performed in implicit solvent using the MM-GBSA method [54,55] as implemented in AMBER14. Data analysis was carried out with OriginLab [56]. Figures were created with PyMOL [57].

2.5.5. Electrostatic potential calculation

The electrostatic potential surface was calculated using the PBSA program from AmberTools with a grid spacing of 1 Å.

2.6. Measurement of HB-EGF release from sHA1 containing hydrogels

HA-AC-coll and HA-AC-/sHA1-AC-coll hydrogels were incubated over night at 37 °C in sterile 2 mL protein LoBind tubes (Eppendorf, Germany) with 200 ng recombinant human HB-EGF in 400 μL Dulbecco's Modified Eagle Medium (DMEM, Biochrom, Germany) supplemented with 5% fetal calf serum (FCS, Biochrom), and 1% ZellShield (Biochrom) on an orbital shaker (*fresh HB-EGF*). After incubation, the supernatant was aliquoted (*HB-EGF after incubation*) and hydrogels were washed 3 times for 10 min with 1 mL DMEM, 5% FCS at 37 °C on an orbital shaker. Gels were incubated with 1 mL DMEM, and 5% FCS for additional 3 days with replacement of medium at each day (*release 24 h, 48 h and 72 h*). Aliquots were stored at −80 °C until use. Volumes of supernatants were determined by weighing. The amount of released HB-EGF was analyzed with human HB-EGF Quantikine ELISA Kit (R&D Systems) according to manufacturer's protocol.

2.7. Cell culture

The investigations were approved by the local ethics committee (269/16-ek) and conducted according to the Declaration of Helsinki Principles (1975).

Human dermal fibroblasts (DF) were obtained from female human breast skin, and porcine DF were isolated from pig ear skin using a tissue dissociating protocol previously described [58]. Dispase II (Roche Diagnostics GmbH, Mannheim, Germany) mediated removal of the epidermal sheet was followed by digestion of the dermal compartment with collagenase (Sigma-Aldrich Chemie GmbH, Germany). To remove tissue debris the cell suspension was passed through 70 μm filters (BD Biosciences, USA). Cells were cultured with DMEM (Biochrom) supplemented with 10% FCS (Biochrom) and 1% ZellShield (Biochrom) at 37 °C, 5% CO_2 until confluence. DF were detached by 0.05% trypsin/0.02% EDTA (Biochrom). For experiments, primary cells between passages 2–4 were used. The human HaCat keratinocyte cell line was purchased from CLS Cell Lines Service GmbH (Germany) and maintained in DMEM supplemented with 10% FCS (Biochrom) and 1% ZellShield (Biochrom).

2.8. Analysis of HaCat cell migration

HaCat cells ($7x10^4$ per well) were seeded in an ImageLock 96 well plate (Essen BioScience, USA) and grown in DMEM supplemented with 10% FCS (Biochrom) and 1% Zellshield (Biochrom). After 3 h medium was changed to DMEM supplemented with 0.5% FCS and cells were cultivated over night at 37 °C, 5% CO_2. Low serum conditions prevent cell proliferation that would otherwise contribute to gap closure.

A 700–800 μm wide scratch was applied in the cell-monolayer with IncuCyte® WoundMaker (Essen BioScience), and remaining cells were washed twice with PBS (Biochrom). Recombinant HB-EGF solutions in DMEM 0.5% FCS (0, 1, 5, 10 and 20 ng/mL) and gel supernatants were added to the cells. Cells were incubated over 24 h-72 h, and migration was determined as closed part of initial wound area every 30 min with IncuCyte® Scratch Wound Cell Migration Software Module (Essen BioScience).

2.9. Analysis of HGF mRNA expression after stimulation of HDF with HB-EGF-containing hydrogel supernatants

Human DF ($4x10^4$ per well) were seeded in a 6 well plate and grown in DMEM supplemented with 10% FCS (Biochrom) and 1% Zellshield (Biochrom). After 4 h, the medium was changed to DMEM supplemented with 5% FCS and cells were cultivated over-night at 37 °C, 5% CO_2. Cells were stimulated with 20 ng/mL HB-EGF (stock solutions) or gel supernatants (release 24 h, 48 h and 72 h) in DMEM 5% FCS for 48 h).

Total RNA was directly prepared from cell cultures with Qiagen RNeasy® Mini Kit (Qiagen, Germany) according to manufacturer's instructions. RNA quantity and purity were determined by spectrophotometry (ND-1000, Nano Drop Technologies, USA). First-strand cDNA synthesis was performed with Superscript Mix (Quantabio, USA) according to manufacturer's instructions by using 0.5–1.0 μg total RNA. GoTaq® qPCR Master Mix (Promega Corporation, USA) with intercalating dye was used for qRT-PCR, which was performed with a Rotor-Gene Q cycler (Qiagen). The primers for human Hepatocyte growth factor (HGF; NM_000601.5; HGFsense: CCACACCGGCACAAATTCTTG; HGF-antisense: AGCCAACTCGGATGTTTGG) and unregulated reference gene 40S ribosomal protein S26 (RPS26; NM_001029) [59]: RPS26sense: CAATGGTCGTGCCAAAAAG, RPS26antisense: TTCACATACAGCTTGGGAAGC were designed and verified with NCBI Primer Blast (https://www.ncbi.nlm.nih.gov/tools/primer-blast) and synthesized by Metabion International AG (Martinsried, Germany). Fluorescence was measured for 20 s at 80–82 °C depending on the melting temperature of amplified DNA. The specificity of PCR product was confirmed one time by sequencing and by melting curve analysis at the end of each run. HGF expression was normalized to the reference gene RPS26.

2.10. Analysis of EGFR signaling

$1,5 \times 10^5$ porcine fibroblasts/well were seeded in 6-well plates and incubated at 37 °C, 5% CO_2 with DMEM/10% FCS (Biochrom) until wells were almost confluent followed by incubation over night with DMEM/0.5% FCS. Cells were washed once with PBS and then incubated for 5 min with recombinant HB-EGF in DMEM (10 ng/mL) or non-diluted supernatants of HB-EGF-exposed HA- and sHA-hydrogels. After 5 min supernatants were completely removed and cells were washed once with cold PBS on ice. Cell extracts were prepared by cooled lysis with a mixture of 10× RIPA-buffer (Cell Signaling Technologies, Germany), 100× Halt™ Phosphatase Inhibitor Cocktail (Thermo Scientific, USA) and 100× Halt™ Protease Inhibitor Cocktail (Thermo Scientific) diluted in aqua dest. Cell lysates were harvested with Cellscraper and briefly sonicated for 30 s with following centrifugation for 10 min at 14,000 g. Protein content was determined with a BCA test (Thermo Scientific). Supernatants were denatured with 5× Laemmli buffer containing β-mercaptoethanol. 15 μg protein/lane was separated by sodium dodecyl sulfate-polyacrylamide gel electrophoresis (TGX Stain-Free™ Protein Gels 4–20%, Biorad, USA) and blotted on nitrocellulose membranes (ProtranTM 0.45 μm GE Healthcare, UK). Activated pAkt was detected by a rabbit anti-phosphoAkt (Ser473) primary antibody (Cell Signaling Technologies (CST), #4060, Germany). Complete Akt was detected after stripping with a rabbit anti Akt antibody (CST, #4691, Germany). Goat-anti-rabbit IRDye® 680RD and goat-anti-rabbit IRDye® 800 (LI-COR Inc., USA) were used as secondary antibodies. Blots were visualized using Odyssey Fc Imaging System (LI-COR Inc). The signals were normalized to the expression of GAP-DH (AB 2302, Merck, Germany).

2.11. Organ culture of porcine skin

Ears from freshly sacrificed pigs were obtained from the Medical-Experimental Center of Leipzig University. Organ culture was set up according to a method described by Brander et al. [60] and slightly modified. After washing the ears for 5 min under running tap water and careful removal of hairs without damaging the epidermal layer, ears were disinfected for 5 min with paper towels soaked in Sterillium (Bode, Germany). Next to rinsing the ears with sterile 0.9% NaCl-solution, *plicae scaphae* were incubated with Betaisodona-solution (Mundipharma, Germany) for 5 min. Excess solution was blotted away with sterile paper towels. Strips of epidermal layer were removed from top of *plicae scaphae* using a sharp razorblade resulting in long epidermal wounds of about 5 mm width. Using a scalpel, cuts were created parallel to the wound margins and whole *plicae* were removed from the underlying adipose tissue. The resulting skin strips were cut into pieces providing rectangular sections (1 cm × 0.5 cm). Rectangular wounds with parallel wound margins were created enabling reproducible microscopic analysis of wound margins in consecutive specimen. The wounded skin pieces were cultured in 12-well plates with dermis down on three layers of sterile gauze soaked with 2 mL of DMEM with 5% FCS (Biochrom). During culture, the epidermis was exposed to the air and the medium contact was given through the dermis.

HA-AC/sHA1-AC/Coll hydrogels were pre-loaded with HB-EGF as described above (see 2.6). After a washing step the hydrogels were placed directly on the wounds overlapping the wound margins. For wounds with solute HB-EGF, 20 μL of stock solution (20 ng/μL; final: 400 ng per wound) were added.

The cultures were incubated at 37 °C for 48 h. Then the wounded skin was fixed in 4% buffered formaldehyde and embedded in paraffin.

2.12. Histological analysis

For histological examination, dewaxed, and rehydrated sections (6 μm thickness) were used. Sections were stained with Masson-Goldner-Trichrome according to manufacturer's protocol (Carl-Roth, Germany) and mounted with Entellan (Merck). Pictures were taken using a Keyence BZ9000 microscope (Keyence, Germany). The length of newly forming epidermis tips was measured with ImageJ [61] on both wound sites, and 8–12 wounds were analyzed per condition. The analysis was performed by two independent investigators (TW & ST).

2.13. Statistics

For statistical significance evaluation, experiments were repeated at least three times. Two-way ANOVA with Bonferroni post-hoc test were used to evaluate differences between groups.

Epidermal tip length was analyzed by one way ANOVA with Fishers LSD Posthoc Test.

P values <0.05 were considered statistically significant.

3. Results

3.1. Analysis of GAG/HB-EGF interaction

The potential interactions of chemically modified HA derivatives with HB-EGF were studied by SPR. Binding analyses showed a concentration-dependent binding of sulfated GAG to immobilized HB-EGF (Fig. 2). sHA1 interacted with HB-EGF stronger than CS at a concentration of 100 μM D.U., while there were no significant differences between both GAG at lower concentrations. No binding was detected for non-sulfated HA at 1 and 10 μM D.U. (Fig. 2B). Native HEP, which served as additional control, showed a binding strength comparable to sHA1 at 100 μM D.U., even though HEP has a higher $D.S._S$ (Fig. 2B). Furthermore, HEP/HB-EGF complexes were less stable than sHA1/HB-EGF complexes as indicated by the much faster dissociation of HEP compared to sHA1 after the end of injection (Fig. 2A).

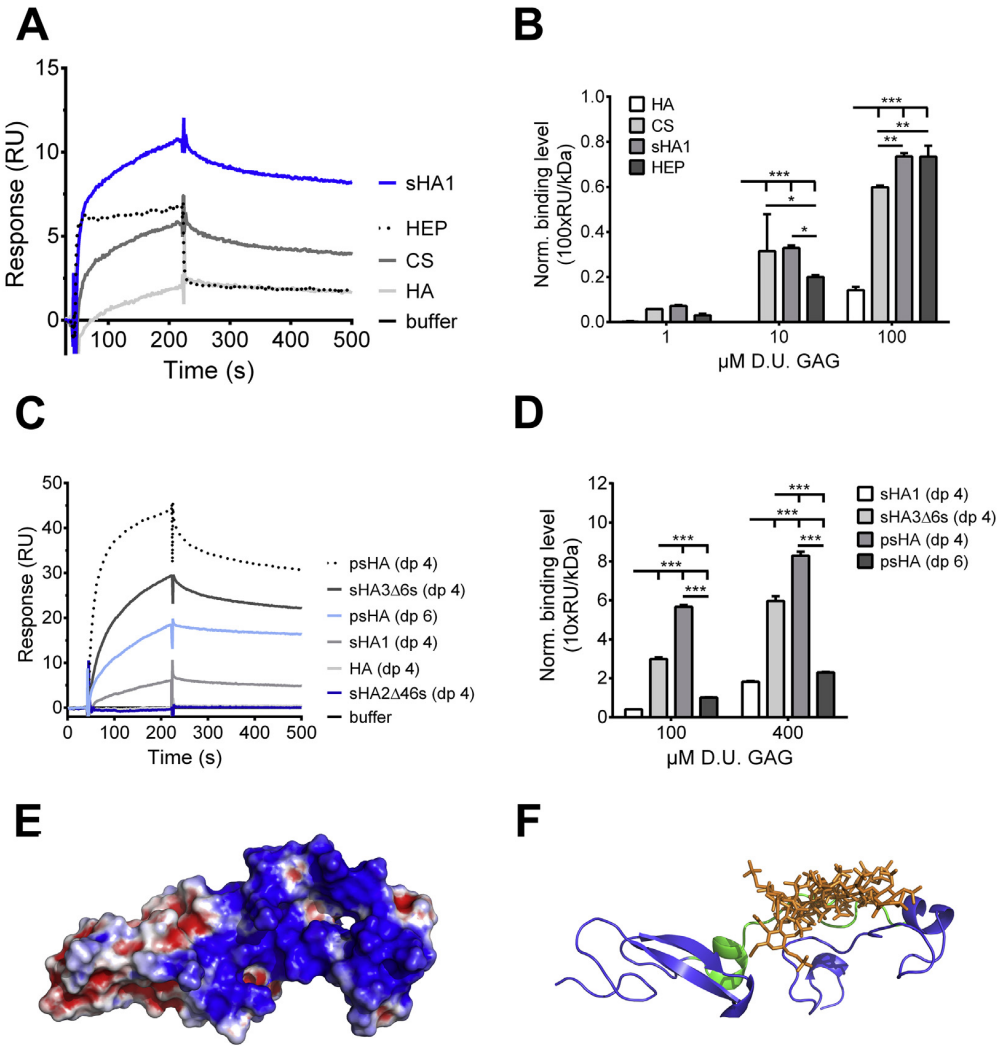

Fig. 2. Interaction of GAG polysaccharides and GAG oligosaccharides with HB-EGF. (A) Binding sensorgrams of 100 μM D.U. native GAG polysaccharides (HA, CS and HEP) and sHA1 to HB-EGF surfaces and (B) normalized binding levels corrected for the molecular weight of the respective GAG. (C) Binding sensorgrams of 400 μM D.U. GAG oligosaccharides to immobilized HB-EGF and (D) normalized binding levels corrected for the molecular weight of the respective GAG. Two-way ANOVA: $^{*}p < 0.05$, $^{**}p < 0.01$, $^{***}p < 0.001$ vs. respective treatment; n = 3. (E) Electrostatic potential surface of the HB-EGF model. Contour color gradients: +5.0 *kT*/*e* (blue) and −5.0 *kT*/*e* (red). (F) Molecular docking results of psHA (dp 4) with HB-EGF. HB-EGF is shown as a blue cartoon with the HB domain in green. psHA (dp 4) is depicted in orange sticks.

For mechanistic studies regarding their interaction with HB-EGF, differently sulfated HA oligosaccharides were analyzed in comparison to native HA-, CS- and HEP-hexasaccharides. Injections of HA (dp4), sHA2Δ46s (dp4) (Fig. 2C and D), CS (dp6), and HEP (dp6) (Fig. S1) did not result in any detectable binding signal. This suggests that longer HEP chains are required for interaction with HB-EGF. In contrast, sHA1 (dp4) which is exclusively sulfated at the C6 position of the *N*-acetylglucosamine, sHA3Δ6s (dp4) and psHA (dp4, dp6) bind HB-EGF in a concentration-dependent manner (Fig. 2D). Except for sHA2Δ46s (dp4), the binding strength of sHA tetrasaccharides increased with the D.S.$_S$.

The molecular recognition of GAG by HB-EGF was further investigated by molecular modeling. The 3D structure of the full HB-EGF protein has not been yet been experimentally resolved and at the PDB there is only a structure available containing a fragment of its C-terminal region which lacks the putative GAG recognition region at the HB domain. Therefore, a combined approach based on threading and comparative modeling techniques was employed in order to build a 3D model of the full structure of solute HB-EGF (86 residues without pro-peptide). Residues D_1-E_{58} (comprising the N-terminal and part of the experimentally resolved C-terminal region) were threaded against a fold library containing all currently available protein structures in order to look for possible structural matches to predict their 3D fold. The best scoring structure obtained (PDB-ID: 1ML4) was taken as template for modeling the N-terminal region. The available structures of a fragment of the C-terminal region of HB-EGF and an EGF-like domain were used as templates for the modeling of the rest of the residues. A refined 3D model of the full structure of HB-EGF was obtained by applying MD simulations (2.5.4). The calculated electrostatic potential of HB-EGF suggested that the N-terminal and HB regions could be involved in GAG binding (Fig. 2E). Molecular docking and MD-based energy analyses indicated that recognition of GAG by HB-EGF takes place precisely on the HB basic patch of the protein (Figs. 2F, S2).

Table 2
MM-GBSA binding free energies obtained for oligohyaluronan derivatives in complex with HB-EGF.

GAG	$\Delta G_{GAG/HB\text{-}EGF}$ (kcal/mol)
psHA (dp4)	−100.9 ± 9.5
sHA3Δ6s (dp4)	−81.8 ± 9.6
psHA (dp6)	−77.5 ± 8.8
sHA1 (dp4)	−34.5 ± 5.5
HA (dp4)	−24.8 ± 4.9

The strength of the computed interaction energies between the investigated GAG and HB-EGF ranked as follows: psHA (dp4) > sHA3Δ6s (dp4) > psHA (dp6) > sHA1 (dp4) > HA (dp4) (Table 2). These results are in agreement with the SPR binding data obtained experimentally (Fig. 2C and D). Considering the studied HA tetrasaccharides, binding increased with higher D.S.S. The interesting weaker binding obtained for psHA (dp6) in comparison to sHA3Δ6s (dp4) and psHA (dp4), in spite of having higher number of sulfate groups, was further investigated. Per-residue free binding energy decomposition analysis revealed that residues R32, K33, K34, K35, K41 and K42 in the HB domain were contributing most in GAG binding (Fig. S3). It is of note that psHA (dp6) showed significantly lower interaction energies with the key residues in comparison to sHA3Δ6s (dp4) and psHA (dp4), which explain the rationale behind the lower binding experimentally observed.

3.2. Release of HB-EGF from hydrogels

In this study we aimed to develop hydrogels that bind and release HB-EGF for their use as wound dressings. For biological validation, the HB-EGF binding and releasing capacity of HA-AC- and sHA1-AC-modified hydrogels and the biological activity of the released HB-EGF were determined.

First, we evaluated the binding and releasing profiles of HA-AC- and sHA1-AC-modified hydrogels loaded with recombinant human HB-EGF (Fig. 3). We could demonstrate that sHA1-AC-containing hydrogels bind 36.7% ± 12.7% of the added HB-EGF, while HA-AC-containing hydrogels captured 28.8% ± 16.1% (Fig. 3A). However, the sHA1-AC-modified hydrogels released significantly less

HB-EGF compared to solely HA-AC modified hydrogels (Fig. 3B). It is of note that also the sHA1-containing hydrogels release approx. 1 ng HB-EGF per 24 h during the observing period of 72 h (Fig. 3B), which might give a suitable local concentration of HB-EGF exerting local biological function.

In order to quantify the established interactions and to shed light on their molecular basis, we performed a computer-based investigation of the binding of HA-AC and sHA1-AC to HB-EGF (Fig. S4) using our molecular models. The calculated interaction energies for the HA and sHA1 acrylate derivatives in complex with HB-EGF (Table 3) were stronger for sHA1-AC than for HA-AC, which is in good agreement with the binding and release data obtained experimentally for the acrylated hydrogels (Fig. 3). In addition, the results obtained from our per-residue energetic contribution analysis indicated more favorable interactions with protein residues K41, K42, and R43 for sHA1-AC than for HA-AC (Fig. S5).

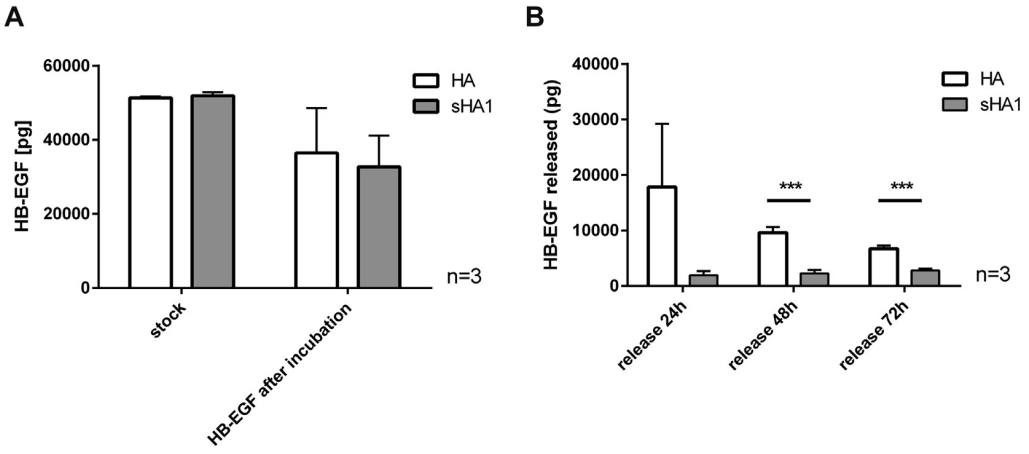

Fig. 3. Binding and release of HB-EGF from HA-AC/sHA1-AC hydrogels: (A) The HB-EGF content was measured before and after the incubation with the hydrogels. Gels were immersed in 200 ng of HB-EGF overnight. (B) The release of recombinant human HB-EGF from hydrogels containing HA-AC or sHA1-AC was quantified per 24 h by ELISA. n = 3, ***p < 0,005.

Table 3
MM-GBSA binding free energies obtained for acrylate hyaluronan derivatives in complex with HB-EGF.

GAG	$\Delta G_{GAG/HB\text{-}EGF}$ (kcal/mol)
HA-AC (dp6)	−16.4 ± 4.7
sHA1-AC (dp6)	−42.2 ± 7.2

3.3. Biological activity of hydrogel released HB-EGF

Based on these interaction studies, we performed an *in vitro* study aiming to investigate the effects of solute HB-EGF on cell types that are essentially involved in wound healing: dermal fibroblasts, a human keratinocyte cell line as well as an organ culture of wounded porcine skin.

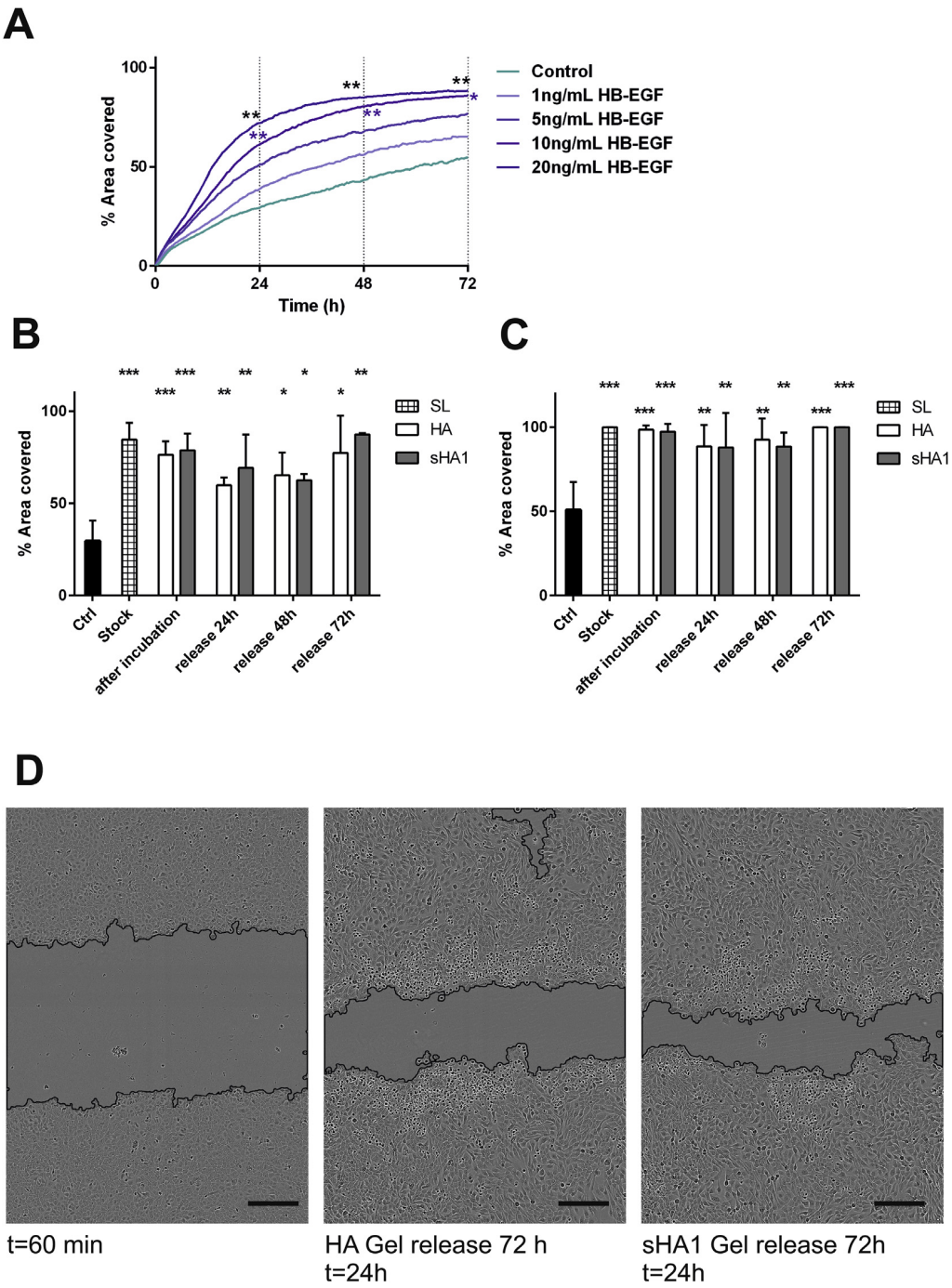

Fig. 4. Recombinant human HB-EGF stimulates keratinocyte migration when added directly (A) as well as after release from HA-AC- or sHA1-AC-containing hydrogels. Scratched HaCat cell monolayers were incubated with HB-EGF (Stock solution, 1–20 ng/mL) (A) or fractions recovered from supernatants of HB-EGF containing hydrogels (B, C). (A) The time course of scratch closure for different concentrations of HB-EGF is shown. (B) represents the cell covered area after 24 h. (C) displays the cell covered area after 72 h. (D) shows representative photographs of scratched wells after 24 h of culture. Bar: 200 μm. ***$p < 0.005$, **$p < 0.01$, *$p < 0.05$ significant changes compared to non-treated HaCat (control), n = 3, 8 wells per condition.

In line with previous findings [18], HB-EGF is able to stimulate migration of a keratinocyte cell line (HaCat) in a concentration-dependent manner. Solute HB-EGF starting from a concentration of 1 ng/mL had a detectable, and from 10 ng/mL a statistically significant effect on cell migration measured by an automated scratch-assay (Fig. 4A).

Next, we evaluated the effects of HB-EGF in supernatants from HA- or sHA1-modified hydrogels. Fractions of supernatants from HA-AC or sHA1-AC containing hydrogels induced HaCat cell migration after 24 h with similar effectiveness compared to a solution of freshly prepared HB-EGF that was used at 5 ng/mL (Fig. 4B and C). Thus, hydrogels containing HA-AC or sHA1-AC release pro-migratory concentrations of HB-EGF for at least 72 h (Fig. 4B–D).

EGFR-signaling is known to induce HGF expression in dermal fibroblasts (DF) [62]. HGF has paracrine activity, stimulating keratinocyte migration and differentiation during wound healing [63] and, thus, it synergizes with HB-EGF. When analyzing the gene expression of HGF in human DF, a significant induction of HGF was detected by recombinant HB-EGF added from stock solutions as well as by HB-EGF released from hydrogels modified with HA-AC or sHA1-ACafter 48 h of exposure (Fig. 5). Strikingly, the binding and release process from the hydrogels did not impair the biological activity detected by comparable induction efficiency as for fresh HB-EGF stock solution (20 ng/mL) (Fig. 5).

As reported previously, HB-EGF exerts its effects by activating EGFR signaling. Upon activation of EGFR by ligands, the MAPKKK/pAkt/cRaf and following the MAPK (ERK1/2/p44/42) signaling pathways can be activated [64]. In a set of experiments we could demonstrate that pre-adsorbed HB-EGF released from loaded HA-AC- or sHA1-AC-modified hydrogels induces EGFR signaling cascade in porcine DF in contrast to empty HA-AC- and sHA1-AC-containing hydrogels. This was visualized and quantitated by detecting activated pAkt (Fig. 6). These phosphorylation events reflect growth factor signaling probably by HB-EGF-activated EGFR and substantiate the bioactivity of HB-EGF released from both HA-AC- and sHA1-AC-containing hydrogels for at least 72 h.

3.4. Gels with sHA1 enhance the effect of HB-EGF on initial epithelial tip expansion

In addition to cell culture experiments, we tested whether HB-EGF bound to sHA1-AC-containing hydrogels is more efficient in supporting keratinocyte proliferation and migration during wound healing than soluble HB-EGF. A porcine skin organ culture model as described by Brandner *et al.* [60] was modified by creating rectangular wounds with a razor blade in order to generate parallel wound margins with fixed initial distance throughout the wound. Wounds were generated in porcine ear skin and the tissue was covered with HA-AC/sHA1/coll hydrogels, which were partially loaded with HB-EGF. After 48 h of culture, wound closure was analyzed by measurement of the lengths of the newly formed epidermal tips (or "migrating epidermal tongue" [65]) (Fig. 7A). Hydrogels containing sHA1-AC loaded with HB-EGF significantly enhanced epidermal tip length compared to unloaded hydrogels and untreated controls (Fig. 7A and B).

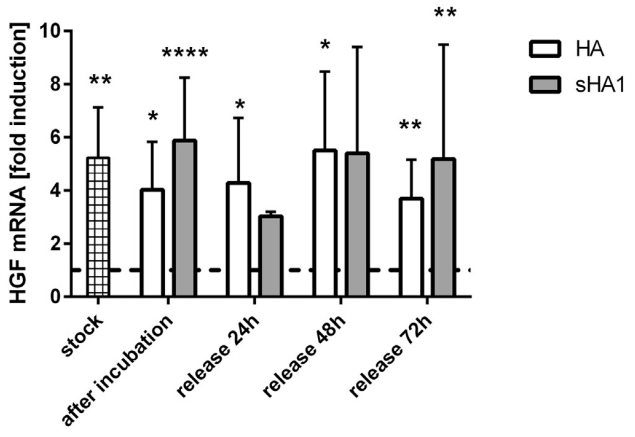

Fig. 5. HB-EGF induces HGF expression in human dermal fibroblasts when added directly as well as after release from HA-AC or sHA1-AC-containing hydrogels. Human DF were incubated for 48 h with HB-EGF solutions released from HA-AC- and HA-AC/ sHA1-AC-containing hydrogels over 24 h, 48 h and 72 h. The HGF expression in untreated fibroblast cultures were set to 1 (dashed line). n = 4; *p < 0.05, **p < 0.01, ****p < 0.0001 unpaired T-test vs. control.

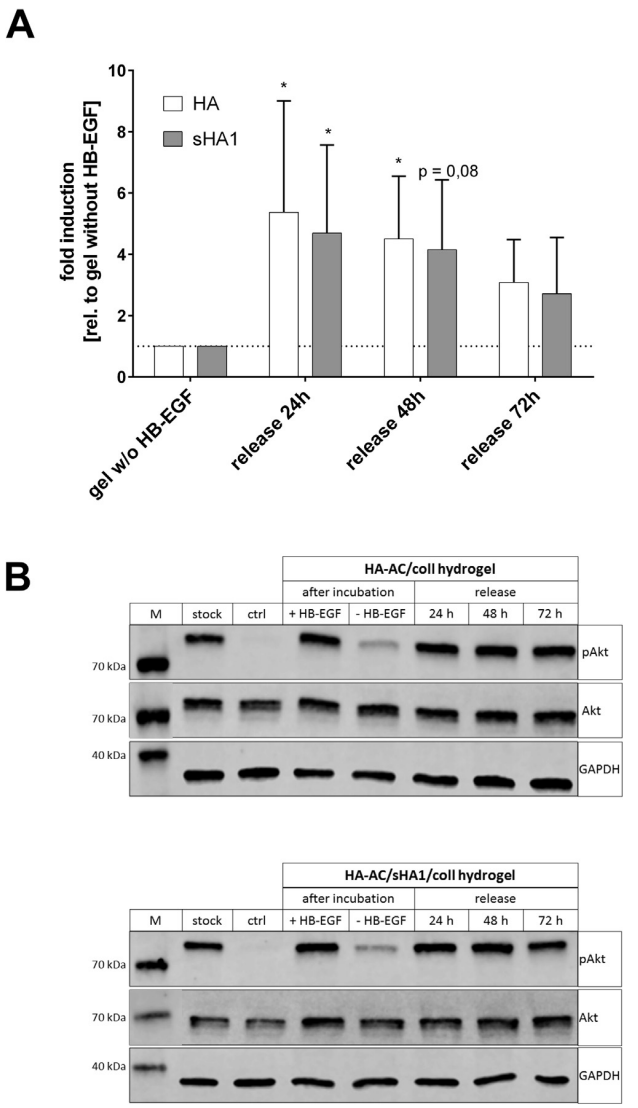

Fig. 6. Induction of Akt-phosphorylation in porcine DF after exposure to HB-EGF released from HA-AC- or sHA1-AC-containing hydrogels. DF were incubated with HB-EGF (stock solution, 10 ng/mL) or fractions recovered from supernatants of HB-EGF containing hydrogels after incubation, 24 h, 48 h and 72 h for 5 min. Signal intensity for phosphorylated Akt was normalized to GAPDH and calculated relatively to control supernatants from empty hydrogels after incubation (*-HB-EGF*). (A) The fold induction of collected data from 3 independent experiments is shown. (B) Representative blots for DF treated with supernatants from HB-EGF loaded HA-AC/coll- (upper panel) and HA-AC/sHA1-AC/coll-hydrogels (lower panel) are shown. M: marker; ctrl: DF starved in 0.5% FCS, n = 3, *p < 0.05.

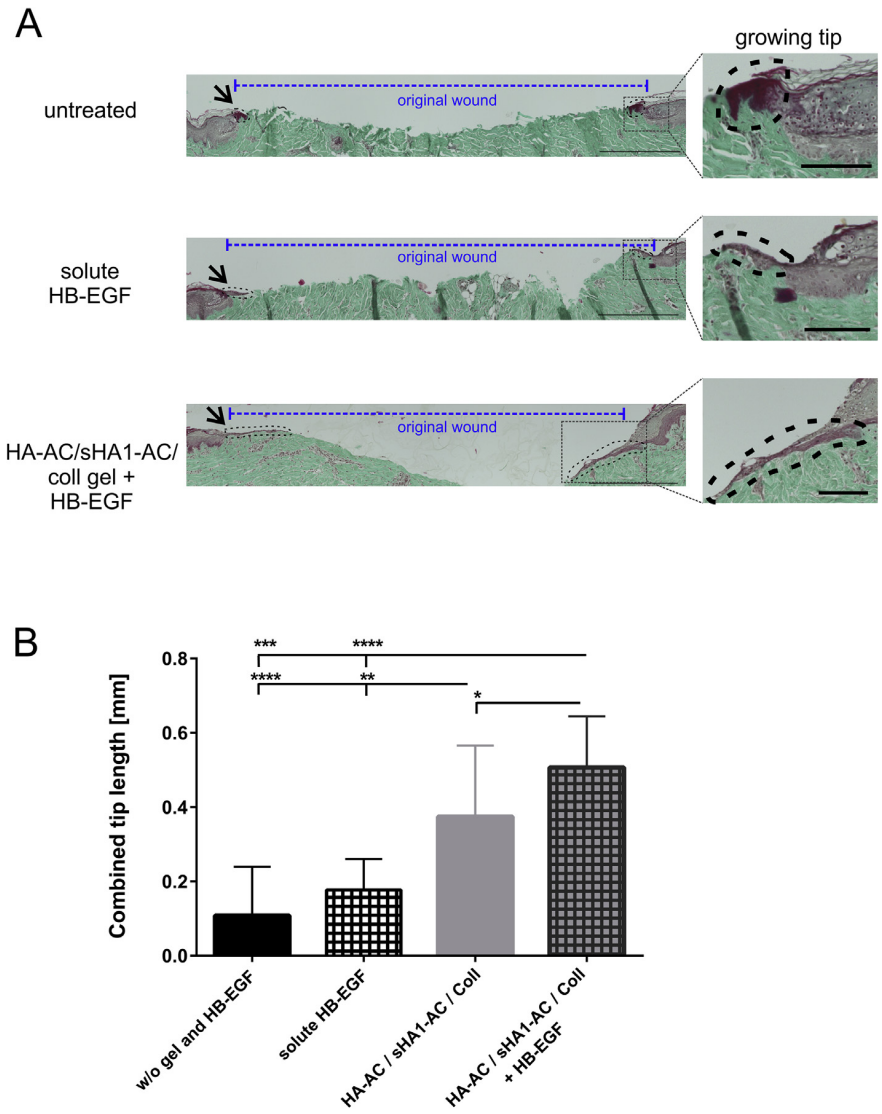

Fig. 7. HB-EGF released from sHA1-AC-containing hydrogels supports epidermal tip formation for wound closure in porcine skin organ culture. sHA1-AC-containing HA-AC/Coll hydrogels were partially loaded with 200 ng HB-EGF per gel and applied for 48 h on experimental wounds of porcine skin. Alternatively, 400 ng solute HBEGF was added directly to the wounds. (A) The epidermal tip length was analyzed by Masson-Goldner Trichrome staining of paraffin sections relative to untreated wounds. Bars: 500 μm (whole wounds); 100 μm (insets). (B) Data on combined tip lengths of both wound sites. n = 3 with 3–4 sections per condition *p < 0.05, **p < 0.01, ***p < 0.005, ****p < 0.001 respectively by one-way ANOVA with Fisher-LSD test.

4. Discussion

The application of recombinant protein mediators is one option to improve disturbed wound healing. Studies with recombinant PDGF demonstrated that very high protein amounts and multiple applications are required. These regimen are cost intensive and the repeated intervention may disturb the healing process [66]. Thus, these mediators have to be immobilized in order to preserve their integrity and function within the reactive wound milieu. Therefore, functional biomaterials that specifically bind and release the bioactive proteins in a controlled manner have to be developed for the topical application on non-healing wounds.

GAG are essential components of the ECM with high biocompatibility. They are often used as constituents in designing biomaterials [1]. The aim of the present study was to improve the bioactivity of HB-EGF, a central mediator of keratinocyte and fibroblast activation during wound healing, by using this reservoir-forming capacity of GAG. Since sulfated HA displayed higher binding to HB-EGF in comparison to HEP and CS, we used the high negative charge content of HA molecules and certain variations of their sulfation pattern for the binding of HB-EGF to HA/collagen-based hydrogels. Moreover, HEP has been shown to display anti-coagulant activity impairing its use in wound treatment [67]. To overcome this problem, sulfate groups have to be removed from HEP resulting in decreased interactions with positively charged mediators [68]. In contrast to HEP, an anti-coagulative activity of sHA derivatives is only reported for those having a sulfation degree above 2.5 per repeating disaccharide unit [67]. Thus, as the degree of sulfation of the incorporated sHA1-AC is significantly below this value, we expect no anti-coagulative effects of the developed hydrogels.

The benefit of introducing negative charges into the molecule was previously reported by the high affinity of HB-EGF toward CS and heparan sulfate proteoglycans [69,70]. Here, sulfation of HA increased its binding to HB-EGF, resulting in comparable binding strength to native CS and HEP. A sulfation-dependent increase of sHA binding was also reported for other growth factors like bone

morphogenetic protein 2 (BMP-2), BMP-4, and transforming growth factor-β1 [32,71,72]. It is of note that only sHA-tetrasaccharides containing at least one sulfate group at C4 or C6 position of the *N*-acetylglucosamine residue were able to interact with HB-EGF. However, the binding response of psHA (dp6) was significantly lower compared to its tetrameric counterpart, indicating an additional influence of the sHA chain length. A similar effect was observed in previous psHA/TIMP-3 interaction studies [33]. There, especially the size and location of HEP-binding regions were identified as factors that determine whether an increased GAG chain length stabilizes or limits the binding to a distinct protein region [73].

The significantly stronger binding obtained for HB-EGF with sHA derivatives compared to HA could be substantiated by theoretical models at atomic detail, thus successfully illustrating the rationale behind the hydrogel system with tunable HB-EGF release profiles. Therefore, sHA1 as GAG derivative based on biotechnologically accessible HA was chosen for hydrogel modification to tune the HB-EGF interaction profiles.

Introduction of sHA1-AC resulted in a slightly increased binding and decreased release of HB-EGF from these hydrogels. Both gel types contain mainly HA-AC (about 95% in case of HA-AC/coll and about 71% in case of HA-AC/sHA1-AC/coll). Thus, differences in their HB-EGF binding capacities may not be significant. Hydrogels containing sHA1-AC did not any display burst release compared to HA-AC-hydrogels, which reflects the strongly increased binding of sHA or sHA-AC derivatives to HB-EGF compared to non-sulfated HA variants as shown by SPR binding and *in silico* studies. The obtained results from HB-EGF release experiments are also in line with previous data showing that the incorporation of sHA1-AC decreases the release of positively charged proteins like lysozyme from hydrogels. This is due to an enhanced electrostatic interaction with negatively charged sulfate groups present in sHA1-AC [28].

sHA1-modified gels controlled the growth factor release in a much stronger manner compared to HB-EGF release studies with HEP-containing crosslinked collagen gels, which were characterized by a quick release of HB-EGF (more than 65% after 48 h) [74]. This is in accordance to our SPR results demonstrating a higher binding strength of sHA1 compared to native HEP, even though the degree of sulfation of sHA1 is lower than that of HEP. It is of note that the sHA1-containing hydrogels release approximately 1 ng of HB-EGF per 24 h during the observing period of 72 h. Thus, there might be a suitable concentration of HB-EGF around the hydrogels that could exert local biological function.

Concerning biological activities of hydrogel-released HB-EGF it was striking that the growth factor released from sHA1-AC-containing hydrogels stimulated HaCat migration as effectively as HB-EGF released from HA-AC/coll hydrogels even though the latter amount of HB-EGF was 2.5–8 fold higher. These results imply that binding of HB-EGF to gels with sHA1 helps to maintain growth factor activity over time. Apparently, the developed hydrogels are able to resemble important properties of the native ECM, which is known to sequester and protect growth factors from degradation by binding to sulfated GAGs [75].

The EGFR downstream signaling is activated during skin wound healing in fibroblasts and keratinocytes [76,77]. Here, HB-EGF released from HA-AC- and sHA1-AC-containing hydrogels effectively activated DF with respect to active signaling (Akt and cRaf phosphorylation), and induction of HGF expression as reported by Niiyama et al. [62]. During wound healing fibroblast-derived HGF exerts paracrine effects on keratinocytes [63]. Thus, activation of EGFR signaling pathways may support wound closure by activating relevant cell types.

Most interestingly, the low concentrations of HB-EGF released from preloaded hydrogels were effective also in wounded organ culture when the proteolytic milieu from the wounded skin was present. Remarkably, the pre-loaded hydrogels releasing HB-EGF (approx. 1–10 ng/mL) were more effective compared to the directly applied HB-EGF solution (400 ng/wound). These findings strongly support the hypothesized benefit of HB-EGF binding to sHA1-AC-containing hydrogels. Likewise, Johnson and Wang reported that the application of 1000 ng HB-EGF in a free form failed to accelerate wound closure in a splinted mouse wound model [18]. In this study high amounts of HB-EGF, stabilized as a coacervate, were required to induce an accelerated healing of full-thickness excisional wounds in mice after 7 or 17 days [18]. Therefore, our and other data demonstrate that reversible immobilization of HB-EGF may strongly improve its local bioavailability and stability in the skin.

Here, we investigated the initial effects on epidermal tip formation after wounding until 48 h post-wounding. Tip formation initially involves mainly keratinocyte migration [78] of both basal and suprabasal keratinocytes supplied by proliferation in the surrounding epidermis [79]. HB-EGF was shown to induce this keratinocyte migration [14,15]. Methodically, longer times of organ culture are accompanied by increasing tissue degradation that would affect analysis. However, future *in vivo* studies will have to show whether the developed hydrogels containing sHA1-AC can be used to promote wound repair of skin tissue.

The fact that the addition of sHA1-containing hydrogels without addition of HB-EGF was effective compared to untreated or solute HB-EGF treated wounds is in line with earlier findings where sulfation of HA alone had beneficial effects on wound repair by enhancing the interaction with proteins and modifying the outcome of inflammation or matrix remodeling [42,68,80]. Here, the modification of the local milieu by so far unknown mechanisms, like stabilization or scavenging of proteins might play a role and is subject of further investigations.

In summary, bioinspired HA/collagen hydrogels containing sHA1-AC reversibly bind HB-EGF and restore its bioactivity to stimulate keratinocytes, fibroblasts, and wound repair. These findings might be translated to biomaterials inducing an improved healing response of injured skin tissues.

5. Conclusion

In this study we proved the hypothesis that introduction of HA or sulfated HA into hydrogels may enable reversible binding of HB-EGF, a mediator that supports wound repair by activating epidermal keratinocytes and dermal fibroblasts. This study was based on the *in silico* modeling of the three-dimensional structure of HB-EGF and the structure-based analysis of its interaction with HA derivatives. Experimental interaction studies, binding and release analysis and different *in vitro* assays and organ culture demonstrate that the introduction of sulfated HA into the hydrogels significantly increases the effectivity of HB-EGF action on target cells. In conclusion, hydrogels functionalized with sulfated HA are promising biomaterials for the development of mediator releasing wound dressings.

Acknowledgements

This study was funded by the Deutsche Forschungsgemeinschaft (DFG, German Research Foundation)– Projektnummer 59307082 – TRR67 (subprojects A3 to VH, DS, A7 to MTP, A8 to JR, B4 to UA, AS, Z3 to MS), the European Regional Development Fund to UA, and instrument resources from the Technical University Dresden, the Leipzig University, and Innovent Jena e.V.

We are grateful for excellent technical assistance by Mrs. A. Majok and Mario Hirt.

Disclosures

The authors declare that they have no competing interests.

Appendix A. Supplementary data

Supplementary data to this article can be found online at https://doi.org/10.1016/j.actbio.2019.01.029.

References

[1] A.R. Im, Y. Park, Y.S. Kim, Isolation and characterization of chondroitin sulfates from sturgeon (Acipenser sinensis) and their effects on growth of fibroblasts, Biol. Pharm. Bull. 33 (2010) 1268–1273, https://doi.org/10.1248/bpb.33.1268.

[2] M. Hemshekhar, R.M. Thushara, S. Chandranayaka, L.S. Sherman, K. Kemparaju, K.S. Girish, Emerging roles of hyaluronic acid bioscaffolds in tissue engineering and regenerative medicine, Int. J. Biol. Macromol. 86 (2016) 917–928, https://doi.org/10.1016/j.ijbiomac.2016.02.032.

[3] J. Lam, N.F. Truong, T. Segura, Design of cell-matrix interactions in hyaluronic acid hydrogel scaffolds, Acta Biomater. 10 (2014) 1571–1580, https://doi.org/10.1016/j.actbio.2013.07.025.

[4] G.D. Prestwich, X.Z. Shu, Y. Liu, S. Cai, J.F. Walsh, C.W. Hughes, S. Ahmad, K.R. Kirker, B. Yu, R.R. Orlandi, A.H. Park, S.L. Thibeault, S. Duflo, M.E. Smith, Injectable synthetic extracellular matrices for tissue engineering and repair, Adv. Exp. Med. Biol. 585 (2006) 125–133.

[5] J. Becher, S. Moeller, M. Schnabelrauch, Building blocks for artificial extracellular matrices based on cross-linkable polysaccharide and glycosaminglycan sulfates, Mater. Sci. Forum. 879 (2016) 1270–1275, https://doi.org/10.4028/www.scientific.net/MSF.879.1270.

[6] C.B. Highley, G.D. Prestwich, J.A. Burdick, Recent advances in hyaluronic acid hydrogels for biomedical applications, Curr. Opin. Biotechnol. 40 (2016) 35–40, https://doi.org/10.1016/j.copbio.2016.02.008.

[7] G. Bhakta, B. Rai, Z.X.H. Lim, J.H. Hui, G.S. Stein, A.J. van Wijnen, V. Nurcombe, G.D. Prestwich, S.M. Cool, Hyaluronic acid-based hydrogels functionalized with heparin that support controlled release of bioactive BMP-2, Biomaterials 33 (2012) 6113–6122, https://doi.org/10.1016/j.biomaterials.2012.05.030.

[8] S.-C. Wu, J.-K. Chang, C.-K. Wang, G.-J. Wang, M.-L. Ho, Enhancement of chondrogenesis of human adipose derived stem cells in a hyaluronan-enriched microenvironment, Biomaterials 31 (2010) 631–640, https://doi.org/10.1016/j.biomaterials.2009.09.089.

[9] Y. Mahalingam, J.T. Gallagher, J.R. Couchman, Cellular adhesion responses to the heparin-binding (HepII) domain of fibronectin require heparan sulfate with specific properties, J. Biol. Chem. 282 (2007) 3221–3230, https://doi.org/10.1074/jbc.M604938200.

[10] H. Habuchi, O. Habuchi, K. Kimata, Sulfation pattern in glycosaminoglycan: does it have a code?, Glycoconj J. 21 (2004) 47–52, https://doi.org/10.1023/B:GLYC.0000043747.87325.5e.

[11] J. Salbach, T.D. Rachner, M. Rauner, U. Hempel, U. Anderegg, S. Franz, J.-C. Simon, L.C. Hofbauer, Regenerative potential of glycosaminoglycans for skin and bone, J. Mol. Med. 90 (2012) 625–635, https://doi.org/10.1007/s00109-011-0843-2.

[12] A. Yu, A. Takeda, K. Kumazawa, H. Miyoshi, M. Kuroyanagi, T. Yoshitake, E. Uchinuma, R. Suzuki, Y. Kuroyanagi, Preliminary clinical study using a novel wound dressing composed of hyaluronic acid and collagen containing EGF, Open J. Regen. Med. 04 (2015) 6–13, https://doi.org/10.4236/ojrm.2015.41002.

[13] E. Iijima, D. Daichi, Toyoda, A. Yamamoto, M. Kuroyanagi, Y. Yoshimitsu Kuroyanagi, In vitro analysis of VEGF and HGF production by fibroblast in cultured dermal substitute combined with EGF-incorporating top dressing, Open J Regen. Med. 03 (2014) 13–21, https://doi.org/10.4236/ojrm.2014.31002.

[14] Y. Su, G.E. Besner, Heparin-binding EGF-like growth factor (HB-EGF) promotes cell migration and adhesion via focal adhesion kinase, J. Surg. Res. 189 (2014) 222–231, https://doi.org/10.1016/j.jss.2014.02.055.

[15] Y. Shirakata, R. Kimura, D. Nanba, R. Iwamoto, S. Tokumaru, C. Morimoto, K. Yokota, M. Nakamura, K. Sayama, E. Mekada, S. Higashiyama, K. Hashimoto, Heparin-binding EGF-like growth factor accelerates keratinocyte migration and skin wound healing, J. Cell Sci. 118 (2005) 2363–2370, https://doi.org/10.1242/jcs.02346.

[16] S.W. Stoll, L. Rittié, J.L. Johnson, J.T. Elder, Heparin-binding EGF-like growth factor promotes epithelial-mesenchymal transition in human keratinocytes, J. Invest. Dermatol. 132 (2012) 2148–2157, https://doi.org/10.1038/jid.2012.78.

[17] M.A. Tolino, E.R. Block, J.K. Klarlund, Brief treatment with heparin-binding EGF-like growth factor, but not with EGF, is sufficient to accelerate epithelial wound healing, Biochim. Biophys. Acta. 1810 (2011) 875–878, https://doi.org/10.1016/j.bbagen.2011.05.011.

[18] N.R. Johnson, Y. Wang, Controlled delivery of heparin-binding EGF-like growth factor yields fast and comprehensive wound healing, J. Control. Release 166 (2013) 124–129, https://doi.org/10.1016/j.jconrel.2012.11.004.

[19] T.J. Puccinelli, P.J. Bertics, K.S. Masters, Regulation of keratinocyte signaling and function via changes in epidermal growth factor presentation, Acta Biomater. 6 (2010) 3415–3425, https://doi.org/10.1016/j.actbio.2010.04.006.

[20] D.M. Beswick, C. Santa Maria, N.F. Ayoub, R. Capasso, P.L. Santa Maria, Epithelial separation theory for post-tonsillectomy secondary hemorrhage: evidence in a mouse model and potential heparin-binding epidermal growth factor-like growth factor therapy, Eur. Arch. Oto-Rhino-Laryngology 275 (2018) 569–578, https://doi.org/10.1007/s00405-017-4810-6.

[21] P.L. Santa Maria, K. Weierich, S. Kim, Y.P. Yang, Heparin binding epidermal growth factor-like growth factor heals chronic tympanic membrane perforations with advantage over fibroblast growth Factor 2 and epidermal growth factor in an animal Model, Otol. Neurotol. 36 (2015) 1279–1283, https://doi.org/10.1097/MAO.0000000000000795.

[22] J. Heo, J.G. Kim, S. Kim, H. Kang, Stat5 phosphorylation is responsible for the excessive potency of HB-EGF, J. Cell. Biochem. 119 (2018) 5297–5307, https://doi.org/10.1002/jcb.26639.

[23] G. Balducci, Stefano, Sacchetti, Massimo, Haxhi, Jonida, Orlando, Giorgio, D'Errico, Valeria, Fallucca, Sara, Menini, Stefano, Pugliese, Physical exercise as therapy for type II diabetes, Diabetes. Metab. Res. Rev. 32 (2014) 13–23, https://doi.org/10.1002/dmrr.

[24] D. Scharnweber, L. Hübner, S. Rother, U. Hempel, U. Anderegg, S.A. Samsonov, M.T. Pisabarro, L. Hofbauer, M. Schnabelrauch, S. Franz, J. Simon, V. Hintze, Glycosaminoglycan derivatives: promising candidates for the design of functional biomaterials, J. Mater. Sci. Mater. Med. 26 (2015) 232, https://doi.org/10.1007/s10856-015-5563-7.

[25] S.A. Thompson, S. Higashiyama, K. Wood, N.S. Pollitt, D. Damm, G. McEnroe, B. Garrick, N. Ashton, K. Lau, N. Hancock, Characterization of sequences within heparin-binding EGF-like growth factor that mediate interaction with heparin, J. Biol. Chem. 269 (1994) 2541–2549. http://www.ncbi.nlm.nih.gov/pubmed/8300582.

[26] S. Higashiyama, J. Abraham, J. Miller, J. Fiddes, M. Klagsbrun, A heparin-binding growth factor secreted by macrophage-like cells that is related to EGF, Science 251 (1991) 936–939, https://doi.org/10.1126/science.1840698.

[27] L. Li, Y. Qian, C. Jiang, Y. Lv, W. Liu, L. Zhong, K. Cai, S. Li, L. Yang, The use of hyaluronan to regulate protein adsorption and cell infiltration in nanofibrous scaffolds, Biomaterials 33 (2012) 3428–3445, https://doi.org/10.1016/j.biomaterials.2012.01.038.

[28] S. Rother, V.D. Galiazzo, D. Kilian, K.M. Fiebig, J. Becher, S. Moeller, U. Hempel, M. Schnabelrauch, J. Waltenberger, D. Scharnweber, V. Hintze, Hyaluronan/collagen hydrogels with sulfated hyaluronan for improved repair of vascularized tissue tune the binding of proteins and promote endothelial cell growth, Macromol. Biosci. 17 (2017) 1–13, https://doi.org/10.1002/mabi.201700154.

[29] R. Kunze, M. Rösler, S. Möller, M. Schnabelrauch, T. Riemer, U. Hempel, P. Dieter, Sulfated hyaluronan derivatives reduce the proliferation rate of primary rat calvarial osteoblasts, Glycoconj. J. 27 (2010) 151–158, https://doi.org/10.1007/s10719-009-9270-9.

[30] S. Köhling, G. Künze, K. Lemmnitzer, M. Bermudez, G. Wolber, J. Schiller, D. Huster, J. Rademann, Chemoenzymatic synthesis of nonasulfated tetrahyaluronan with a paramagnetic tag for studying its complex with interleukin-10, Chem. - A Eur. J. 22 (2016) 5563–5574, https://doi.org/10.1002/chem.201504459.

[31] S. Köhling, J. Blaszkiewicz, G. Ruiz-Gómez, M.I. Fernández-Bachiller, K. Lemmnitzer, N. Panitz, A.G. Beck-Sickinger, J. Schiller, M.T. Pisabarro, J. Rademann, Syntheses of defined sulfated oligohyaluronans reveal structural effects, diversity and thermodynamics of GAG–protein binding, Chem. Sci. (2019), https://doi.org/10.1039/C8SC03649G.

[32] V. Hintze, S. Moeller, M. Schnabelrauch, S. Bierbaum, M. Viola, H. Worch, D. Scharnweber, Modifications of hyaluronan influence the interaction with human bone morphogenetic protein-4 (hBMP-4), Biomacromolecules 10 (2009) 3290–3297, https://doi.org/10.1021/bm9008827.

[33] S. Rother, S.A. Samsonov, S. Moeller, M. Schnabelrauch, J. Rademann, J. Blaszkiewicz, S. Köhling, J. Waltenberger, M.T. Pisabarro, D. Scharnweber, V. Hintze, Sulfated hyaluronan alters endothelial cell activation *in vitro* by controlling the biological activity of the angiogenic factors vascular endothelial growth factor-a and tissue inhibitor of metalloproteinase-3, ACS Appl. Mater. Interfaces. 9 (2017) 9539–9550, https://doi.org/10.1021/acsami.7b01300.

[34] M.J. Sippl, Boltzmann's principle, knowledge-based mean fields and protein folding. An approach to the computational determination of protein structures, J. Comput. Aided Mol. Des. 7 (1993) 473–501.

[35] M.J. Sippl, S. Weitckus, Detection of native-like models for amino acid sequences of unknown three-dimensional structure in a data base of known protein conformations, Proteins 13 (1992) 258–271, https://doi.org/10.1002/prot.340130308.

[36] M.T. Pisabarro, B. Leung, M. Kwong, R. Corpuz, G.D. Frantz, N. Chiang, R. Vandlen, L.J. Diehl, H.S. Kim, D. Eaton, K.N. Schmidt, Cutting edge: novel human dendritic cell- and monocyte-attracting chemokine-like protein identified by fold recognition methods, J. Immunol. 176 (2006) 2069–2073, https://doi.org/10.4049/jimmunol.176.4.2069.

[37] Discovery Studio Modeling Environment, Release 3.5, Accelrys Software Inc., (2012).

[38] S. Van Boxstael, R. Cunin, S. Khan, D. Maes, Aspartate transcarbamylase from the hyperthermophilic archaeon Pyrococcus abyssi: thermostability and 1.8A resolution crystal structure of the catalytic subunit complexed with the bisubstrate analogue N-phosphonacetyl-L-aspartate, J. Mol. Biol. 326 (2003) 203–216, https://doi.org/10.1016/S0022-2836(02)01228-7.

[39] G.V. Louie, W. Yang, M.E. Bowman, S. Choe, Crystal structure of the complex of diphtheria toxin with an extracellular fragment of its receptor, Mol. Cell. 1 (1997) 67–78, https://doi.org/10.1016/S1097-2765(00)80008-8.

[40] D.A. Case, J.T. Berryman, R.M. Betz, D.S. Cerutti, I.T. Cheatham, T.A. Darden, R.E. Duke, T.J. Giese, H. Gohlke, A.W. Goetz, N. Homeyer, S. Izadi, P. Janowski, A. Kovalenko, T.S. Lee, S. LeGrand, P. Li, T. Luchko, R. Luo, B. Madej, K.M. Merz, G. Monard, P. Needham, H. Nguyen, H.T. Nguyen, I. Omelyan, A. Onufriev, D.R. Roe, A. Roitberg, R. Salomon-Ferrer, C.L. Simmerling, W. Smith, J. Swails, R.C. Walker, J. Wang, R.M. Wolf, X. Wu, D.M. York, P.A. Kollmann, AMBER 2014 (2014).
[41] Molecular Operating Environment (MOE), version 2016; Chemical Computing Group Inc.: Montreal, QC, Canada (2016)., (n.d.).
[42] A. van der Smissen, S. Samsonov, V. Hintze, D. Scharnweber, S. Moeller, M. Schnabelrauch, M.T. Pisabarro, U. Anderegg, Artificial extracellular matrix composed of collagen I and highly sulfated hyaluronan interferes with TGFβ1 signaling and prevents TGFβ1-induced myofibroblast differentiation, Acta Biomater. 9 (2013) 7775–7786, https://doi.org/10.1016/j.actbio.2013.04.023.
[43] G.M. Morris, D.S. Goodsell, R.S. Halliday, R. Huey, W.E. Hart, R.K. Belew, A.J. Olson, Automated docking using a Lamarckian genetic algorithm and an empirical binding free energy function, J. Comput. Chem. 19 (1998) 1639–1662, https://doi.org/10.1002/(SICI)1096-987X(19981115)19:14<1639::AID-JCC10>3.0.CO;2-B.
[44] M. Ester, H.-P. Kriegel, J. Sanders, X. Xu, A density-based algorithm for discovering clusters in large spatial databases with noise, Proc. 2nd Int. Knowl. Discov. Data Min. (1996) 226–231. 10.1.1.121.9220.
[45] J.-P. Gehrcke, M.T. Pisabarro, Identification and characterization of a glycosaminoglycan binding site on interleukin-10 via molecular simulation methods, J. Mol. Graph. Model. 62 (2015) 97–104, https://doi.org/10.1016/j.jmgm.2015.09.003.
[46] K.N. Kirschner, A.B. Yongye, S.M. Tschampel, J. González-Outeiriño, C.R. Daniels, B.L. Foley, R.J. Woods, GLYCAM06: a generalizable biomolecular force field. Carbohydrates, J. Comput. Chem. (2008) 622–655, https://doi.org/10.1002/jcc.20820. 29.
[47] C.J.M. Huige, C. Altona, Force-field parameters for sulfates and sulfamates based on Ab-initio calculations – extensions of amber and charmm fields, J. Comput Chem. 16 (1995) 56–79.
[48] R.C. Walker, M.F. Crowley, D.A. Case, The implementation of a fast and accurate QM/MM potential method in Amber, J. Comput. Chem. 29 (2008) 1019–1031, https://doi.org/10.1002/jcc.20857.
[49] C.I. Bayly, P. Cieplak, W. Cornell, P.A. Kollman, A well-behaved electrostatic potential based method using charge restraints for deriving atomic charges: the RESP model, J. Phys. Chem. 97 (1993) 10269–10280, https://doi.org/10.1021/j100142a004.
[50] F.-Y. Dupradeau, A. Pigache, T. Zaffran, C. Savineau, R. Lelong, N. Grivel, D. Lelong, W. Rosanski, P. Cieplak, The R.E.D. tools: advances in RESP and ESP charge derivation and force field library building, Phys. Chem. Chem. Phys. 12 (2010) 7821–7839, https://doi.org/10.1039/c0cp00111b.
[51] M.J. Frisch, G.W. Trucks, H.B. Schlegel, G.E. Scuseria, M.A. Robb, J.R. Cheeseman, G. Scalmani, V. Barone, B. Mennucci, G.A. Petersson, H. Nakatsuji, M. Caricato, X. Li, H.P. Hratchian, A.F. Izmaylov, J. Bloino, G. Zheng, J.L. Sonnenberg, M. Hada, M. Ehara, K. Toyota, R. Fukuda, J. Hasegawa, M. Ishida, T. Nakajima, Y. Hona, O. Kitao, H. Nakaj, T. Vreven, J.A. Montgomery Jr., J.E. Peralta, F. Ogliaro, M.J. Bearpark, J. Heyd, E.N. Brothers, K.N. Kudin, V.N. Staroverov, R. Kobayashi, J. Normand, K. Raghavachari, A.P. Rendell, J.C. Burant, S.S. Iyengar, J. Tomasi, N. Cossi, N. Rega, N.J. Millam, M. Klene, J.E. Knox, J.B. Cross, V. Bakken, C. Adamo, J. Jaramillo, R. Gomperts, R.E. Stratmann, O. Yazyev, A.J. Austin, R. Cammi, C. Pomelli, J.W. Ochterski, R.L. Martin, K. Morokuma, V.G. Zakrzewski, P. Voth, G. A. Salvador, J.J. Dannenberg, S. Dapprich, A.D. Daniels, Ö. Farkas, J.B. Foresman, J.V. Ortiz, J. Cioslowski, F. D.J., Gaussian 09, Revision C.01, (2009). http://gaussian.com/glossary/g09/ (accessed August 22, 2018).
[52] J.M. Wang, R.M. Wolf, J.W. Caldwell, P.A. Kollman, D.A. Case, Development and testing of a general amber force field, J. Comput. Chem. 25 (2004) 1157–1174.
[53] W. Humphrey, A. Dalke, K. Schulten, VMD: visual molecular dynamics, J. Mol. Graph. 14 (1996) 33–38, https://doi.org/10.1016/0263-7855(96)00018-5.
[54] J. Wang, P. Morin, W. Wang, P.A. Kollman, Use of MM-PBSA in reproducing the binding free energies to HIV-1 RT of TIBO derivatives and predicting the binding mode to HIV-1 RT of efavirenz by docking and MM-PBSA, J. Am. Chem. Soc. 123 (2001) 5221–5230, https://doi.org/10.1021/ja003834q.
[55] B.R. Miller, T.D. McGee, J.M. Swails, N. Homeyer, H. Gohlke, A.E. Roitberg, MMPBSA.py: an efficient program for end-state free energy calculations, J. Chem. Theory Comput. 8 (2012) 3314–3321, https://doi.org/10.1021/ct300418h.
[56] OriginLab, Northampton, MA, available: http://www.originlab.com, Origin2018b., (n.d.).
[57] L.L. Schrödinger, The PyMOL Molecular Graphics System, Version 1.8 (2009-2015), (n.d.).
[58] A. Saalbach, C. Klein, C. Schirmer, W. Briest, U. Anderegg, J.C. Simon, Dermal fibroblasts promote the migration of dendritic cells, J. Invest. Dermatol. 130 (2010) 444–454, https://doi.org/10.1038/jid.2009.253.
[59] S. Vincent, L. Marty, P. Fort, S26 ribosomal protein RNA: an invariant control for gene regulation experiments in eucaryotic cells and tissues, Nucleic Acids Res. 21 (1993) 1498.
[60] J.M. Brandner, S. Zacheja, P. Houdek, I. Moll, R. Lobmann, Expression of matrix metalloproteinases, cytokines, and connexins in diabetic and nondiabetic human keratinocytes before and after transplantation into an ex vivo wound-healing model, Diabetes Care 31 (2008) 114–120, https://doi.org/10.2337/dc07.
[61] C.T. Rueden, J. Schindelin, M.C. Hiner, B.E. DeZonia, A.E. Walter, E.T. Arena, K.W. Eliceiri, Image J2: ImageJ for the next generation of scientific image data, BMC Bioinform. 18 (2017) 529, https://doi.org/10.1186/s12859-017-1934-z.
[62] H. Niiyama, Y. Kuroyanagi, Development of novel wound dressing composed of hyaluronic acid and collagen sponge containing epidermal growth factor and vitamin C derivative, J. Artif. Organs. 17 (2014) 81–87, https://doi.org/10.1007/s10047-013-0737-x.
[63] M.A. Seeger, A.S. Paller, The roles of growth factors in keratinocyte migration, Adv. Wound Care. 4 (2015) 213–224, https://doi.org/10.1089/wound.2014.0540.
[64] S. Akhtar, M.H.M. Yousif, B. Chandrasekhar, I.F. Benter, Activation of EGFR/ERBB2 via pathways involving ERK1/2, P38 MAPK, AKT and FOXO enhances recovery of diabetic hearts from ischemia-reperfusion injury, PLoS One. 7 (2012), https://doi.org/10.1371/journal.pone.0039066 e39066.
[65] A.F. Laplante, L. Germain, F.A. Auger, V. Moulin, Mechanisms of wound reepithelialization: hints from a tissue-engineered reconstructed skin to long-standing questions, FASEB J. 15 (2001) 2377–2389, https://doi.org/10.1096/fj.01-0250com.
[66] T.A. Mustoe, A Phase II study to evaluate recombinant platelet-derived growth factor-BB in the treatment of stage 3 and 4 pressure ulcers, Arch. Surg. 129 (1994) 213–219, https://doi.org/10.1001/archsurg.1994.01420260109015.
[67] A. Magnani, S. Lamponi, R. Rappuoli, R. Barbucci, Sulphated hyaluronic acids: a chemical and biological characterisation, Polym. Int. 46 (1998) 225–240, https://doi.org/10.1002/(SICI)1097-0126(199807)46:3<225::AID-PI45>3.3.CO;2-9.
[68] N. Lohmann, L. Schirmer, P. Atallah, E. Wandel, R.A. Ferrer, C. Werner, J.C. Simon, S. Franz, U. Freudenberg, Glycosaminoglycan-based hydrogels capture inflammatory chemokines and rescue defective wound healing in mice, Sci. Transl. Med. 9 (2017) eaai9044, https://doi.org/10.1126/scitranslmed.aai9044.
[69] C.L. Chu, A.L. Goerges, M.A. Nugent, Identification of common and specific growth factor binding sites in heparan sulfate proteoglycans, Biochemistry 44 (2005) 12203–12213, https://doi.org/10.1021/bi050241p.
[70] C.D. Nandini, T. Mikami, M. Ohta, N. Itoh, F. Akiyama-Nambu, K. Sugahara, Structural and functional characterization of oversulfated chondroitin sulfate/dermatan sulfate hybrid chains from the notochord of hagfish: Neuritogenic and binding activities for growth factors and neurotrophic factors, J. Biol. Chem. 279 (2004) 50799–50809, https://doi.org/10.1074/jbc.M404746200.
[71] V. Hintze, S.A. Samsonov, M. Anselmi, S. Moeller, J. Becher, M. Schnabelrauch, D. Scharnweber, M.T. Pisabarro, Sulfated glycosaminoglycans exploit the conformational plasticity of bone morphogenetic protein-2 (BMP-2) and alter the interaction profile with its receptor, Biomacromolecules 15 (2014) 3083–3092, https://doi.org/10.1021/bm5006855.
[72] V. Hintze, A. Miron, S. Moeller, M. Schnabelrauch, H.P. Wiesmann, H. Worch, D. Scharnweber, Sulfated hyaluronan and chondroitin sulfate derivatives interact differently with human transforming growth factor-beta1 (TGF-beta1), Acta Biomater. 8 (2012) 2144–2152.
[73] S. Rother, S.A. Samsonov, T. Hofmann, J. Blaszkiewicz, S. Köhling, S. Moeller, M. Schnabelrauch, J. Rademann, S. Kalkhof, M. von Bergen, M.T. Pisabarro, D. Scharnweber, V. Hintze, Structural and functional insights into the interaction of sulfated glycosaminoglycans with tissue inhibitor of metalloproteinase-3 – a possible regulatory role on extracellular matrix homeostasis, Acta Biomater. 45 (2016) 143–154, https://doi.org/10.1016/j.actbio.2016.08.030.
[74] M.A. Princz, H. Sheardown, Heparin-modified dendrimer crosslinked collagen matrices for the delivery of heparin-binding epidermal growth factor, J. Biomed. Mater. Res. – Part A. 100 A (2012) 1929–1937, https://doi.org/10.1002/jbm.a.34128.
[75] G.S. Schultz, A. Wysocki, Interactions between extracellular matrix and growth factors in wound healing, Wound Repair Regen. 17 (2009) 153–162, https://doi.org/10.1111/j.1524-475X.2009.00466.x.
[76] J. Yin, K. Xu, J. Zhang, A. Kumar, F.-S.X. Yu, Wound-induced ATP release and EGF receptor activation in epithelial cells, J. Cell Sci. 120 (2007) 815–825, https://doi.org/10.1242/jcs.03389.
[77] K. Ehrenreiter, D. Piazzolla, V. Velamoor, I. Sobczak, J.V. Small, J. Takeda, T. Leung, M. Baccarini, Raf-1 regulates Rho signaling and cell migration, J. Cell Biol. 168 (2005) 955–964, https://doi.org/10.1083/jcb.200409162.
[78] Y. Poumay, C.L. de Rouvroit, HB-EGF, the growth factor that accelerates keratinocyte migration, but slows proliferation, J. Invest. Dermatol. 132 (2012) 2129–2130, https://doi.org/10.1038/JID.2012.225.
[79] K. Safferling, T. Sütterlin, K. Westphal, C. Ernst, K. Breuhahn, M. James, D. Jäger, N. Halama, N. Grabe, Wound healing revised: a novel reepithelialization mechanism revealed by in vitro and in silico models, J. Cell Biol. 203 (2013) 691–709, https://doi.org/10.1083/jcb.201212020.
[80] S.A. Muller, A. van der Smissen, M. von Feilitzsch, U. Anderegg, S. Kalkhof, M. von Bergen, Quantitative proteomics reveals altered expression of extracellular matrix related proteins of human primary dermal fibroblasts in response to sulfated hyaluronan and collagen applied as artificial extracellular matrix, J. Mater. Sci. Mater. Med. 23 (2012) 3053–3065, https://doi.org/10.1007/s10856-012-4760-x.